Pure and Applied Geophysics



Effect of Vortex Initialization and Relocation Method in Anticipating Tropical Cyclone Track and Intensity over the Bay of Bengal

RAGHU NADIMPALLI, KRISHNA K. OSURI, DU. C. MOHANTY, A. K. DAS, and DEV NIYOGI

Abstract—This study assessed two different vortex initialization (VI) and relocation methods for improved prediction of tropical cyclones (TCs) over the Bay of Bengal (BoB) using the triply nested (27/9/3 km) state-of-the-art Hurricane Weather Research and Forecasting (HWRF) model. The first VI method, "cold-start," obtained the initial TC vortex from the global analysis. The second one, "cyclic-start," received the initial vortex from the 6-h forecast of the previous forecast cycle of the same model. In both the strategies, the vortex was corrected to the position, strength, and structure defined by the India Meteorological Department. A total of 32 forecast cases (from five cyclones) over the BoB were considered. The cyclic-start experiments yielded better initial structure and asymmetry as compared to the coldstart experiments. The average statistics indicated that the cyclic initialization improved the 24-h track prediction (by 29%), while the cold initialization was better for the 72-h prediction (by \sim 28%). The intensity was consistently improved in the cyclic-start experiment by up to 68%. The number of cyclic initializations depended on the TC duration. On average, the cyclic initialization improved the representation (strength and size) of the initial vortex up to nine cycles after the first cold start and exhibited an improved skill of 25%; beyond nine cycles, the skill improvement was only 12%. Diagnostic analyses of very severe cyclonic storm (VSCS) Phailin (rapidly intensified) and VSCS Lehar (rapidly weakening) revealed that the cyclic initialization realistically represented equivalent potential temperature, upper-level cloud condensate, and moisture intrusion, which improved the model performance. This study brought out the benefit of the (cyclic) VI for improved TC prediction capabilities in the BoB basin.

Supplementary Information The online version contains supplementary material available at https://doi.org/10.1007/s00024-021-02815-x.

Keywords: Vortex initialization, HWRF model, tropical cyclones, Bay of Bengal.

1. Introduction

Numerical weather prediction (NWP) is an initial value problem, which requires realistic initial conditions (IC) to produce more accurate predictions (Kreiss and Lorenz, 2004). The generation of highquality IC is particularly significant for tropical cyclone (TC) prediction, as TCs often develop in the open seas where the data is limited. The scarcity of observations over the North Indian Ocean (NIO), including the Bay of Bengal (BoB) and the Arabian Sea (AS), results in an initial TC vortex with a large average position error (~ 61 km) and intensity error (-15 knots) (Osuri et al., 2013). Recent studies have considered (i) enhanced resolution (Osuri et al., 2013; Mohanty et al., 2019), (ii) data assimilation of conventional and nonconventional observations such as satellite-derived winds (Osuri et al., 2012; Singh et al., 2008), Doppler weather radar observations (Osuri et al., 2015), and satellite radiance data (Nadimpalli et al., 2020; Routray et al., 2016; Sandeep et al., 2006; Singh et al., 2012) to improve the simulation of TCs over the NIO basin. There is a growing availability of observational data around TCs with remote sensing technology (mainly through satellites and Doppler radar). Despite these advances, accurate initial TC position, intensity, and structures are still elusive.

State-of-the-art TC models improve the vortex representation in the initial analyses through various vortex initialization (VI) and relocation methods. Past studies have demonstrated that the VI and relocation

School of Earth Ocean and Climate Sciences, Indian Institute of Technology Bhubaneswar, Bhubaneswar, Odisha, India.

² Department of Earth and Atmospheric Sciences, National Institute of Technology Rourkela, Rourkela, Odisha, India. E-mail: osurikishore@gmail.com

Numerical Weather Prediction Division, India Meteorological Department, New Delhi, India.

⁴ Department of Geological Sciences, Jackson School of Geosciences, and Department of Civil, Architectural, and Environmental Engineering, University of Texas at Austin, Austin, TX 78712, USA.

method improved initial TC vortex in terms of position, intensity, and structure over global oceans (Leslie & Holland, 1995; Davis & Low-Nam, 2001; Pu & Braun, 2001; Kwon & Cheong, 2010; Gopalakrishnan et al., 2012; Zou et al., 2015) as well as over the NIO basin (Busireddy et al., 2019; Das et al., 2015; Mohanty et al., 2013; Osuri et al., 2017). Some advantages of VI are the ability to customize the vortex structure and the low computational cost in terms of time and power. The success noted in earlier initialization studies, which used a bogus vortex, varies from case to case due to the inconsistency of the vortex against the characteristics of the prediction model (Iwasaki et al., 1987; Kurihara et al., 1990; Leslie & Holland, 1995; Lord, 1991; Mathur, 1991; Trinh & Krishnamurti, 1992; Wang, 1998). Kurihara et al. (1993) introduced a consistent dynamic initialization method involving an idealized model to generate a realistic vortex with the nudging of the pressure and wind components towards a structural match with observations. Hendricks et al. (2011) employed a technique in which the TC initial vortex removed from the initial analyses was merged with an idealized vortex nudged towards observed surface pressure and winds. Cha and Wang (2013) used a sixhourly cycle with a warm experiment model forecast initialization to produce a more accurate TC boundary layer and an unbalanced secondary circulation in the initial condition.

Many NWP centers use a bogus scheme that forces a TC vortex into the numerical analysis at the initial time. These bogus mechanisms vary with the various NWP centers, but typically include a symmetric vortex with some auxiliary asymmetry to account for the TC movement and the environmental flow. Three types of bogus techniques are broadly used in operational models (Peng et al., 1993): (i) adding bogus observational data before objective analysis as used in the National Centers for Environmental Prediction (NCEP) Global Forecast System (GFS) model (Lord, 1991) and the UK Meteorological Office (UKMO) global model (Heming et al., 1995); (ii) adding a more composite vortex circulation demarcated by an analytical expression after the objective analysis but before model initialization as used in the Japan Meteorological Agency (JMA) typhoon model (Ueno, 1995) and the quasi-Lagrangian model (QLM) (Mathur, 1991, Prasad & Rao, 2003); and (iii) bogusing a "spinup" vortex produced by the same forecast model, in place of using an analytical one, for example, in the Geophysical Fluid Dynamics Laboratory (GFDL) TC model (Kurihara et al. 1995) and Taiwan's Central Weather Bureau (CWB)-based Typhoon-Track Forecast System (TFS) (Peng et al., 1993). It is noted that even for the same model, both the horizontal and vertical structures of the axisymmetric vortex vary among the operational centers with different methods.

The state-of-the-art cloud-resolving Hurricane Weather Research and Forecasting (HWRF) model is recognized for its overall good performance over global oceans (Tallapragada, 2016) as well as over the NIO basin (Das et al., 2015; Mohanty et al., 2015; Nadimpalli et al., 2019; Osuri et al., 2017). This model is now operational for TC forecasting at the India Meteorological Department (IMD), New Delhi. Hence, the HWRF model is considered in this study to demonstrate the credibility of VI strategies viz. cold-start VI and cyclic-start VI in the HWRF system. The study also evaluates the maximum number of cycles (cyclic experiments) that could provide better forecast guidance in the life span of TCs. A total of 32 cases from five recent TCs over BoB are analyzed. A summary of these TCs (number of forecasts, nature of TC, vortex depth) is given in Table 1.

2. Data and Methodology

The HWRF modeling system uses a non-hydrostatic mesoscale model (NMM) dynamic core with rotated latitude–longitude projection and E-grid staggering. The 2014 version of the HWRF (v3.5a) was applied in this study. The model was configured with two moving nests that follow the TC vortex throughout the integration. An outermost static domain (D01) of about $80^{\circ} \times 80^{\circ}$ (long × lat) size with a horizontal grid spacing of ~ 27 km and 42 vertical levels was configured over the NIO region around the TC center. Two inner nested domains of size $\sim 11^{\circ} \times 10^{\circ}$ (D02) and $\sim 7.2^{\circ} \times 6.5^{\circ}$ (D03) were used at 9 km and 3km grid spacing,

Table 1
Summary of the storms considered in the present study

Case no.	Storm name (feature)	Initial conditions	Forecast length (h)	Vortex depth	Remarks			
1	VSCS Nargis (Recurved)	12:00 UTC 27 April 2008	132	Shallow	One of the most devastating TCs of the BoB in recent years, with over 138,000 fatalities. The storm formed under the influence of active inter-tropical convergence zone over southeast BoB. While moving northwestward initially, it recurved northeastward and made landfall			
2	,	00:00 UTC 28 April 2008	120	Shallow				
3		12:00 UTC 28 April 2008	108	Moderate	over the Myanmar coast. It exhibited rapid intensification (RI) during 27–28 April 2008			
4		00:00 UTC 29 April 2008	96	Moderate				
5		12:00 UTC 29 April 2008	84	Deep				
6		00:00 UTC 30 April 2008	72	Deep				
7	VSCS Phailin (Straight-	12:00 UTC 09 October 2013	84		Second most intense TC of the BoB after the Orissa Super Cyclone (1999). The system first initiated as a depression on 4 October 2013,			
8	moving)	00:00 UTC 10 October 2013	72	Moderate	over the Gulf of Thailand. While moving westward, the storm emerged into the BoB. It underwent a RI (~ 70 knots change in 24 h) and made			
9		12:00 UTC 10 October 2013	60	Deep	landfall over Gopalpur, Orissa			
10 11		00:00 UTC 11 October 2013 12:00 UTC 11	48 36	Deep				
12		October 2013 00:00 UTC 12	24	Deep Deep				
13	SCS Helen	October 2013 12:00 UTC 19	84	•	TC Helen appeared as a low-pressure system on 18 November 2013 over			
13	(Straight- moving)	November 2013	04	Wioderate	central BoB and deepened into a deep depression on 19 November 2013. While moving northwestward, it intensified into an SCS. Helen			
14		00:00 UTC 20 November 2013	72	Moderate	made landfall over the Machilipatnam coast of Andhra Pradesh			
15		12:00 UTC 20 November 2013	60	Moderate				
16		00:00 UTC 21 November 2013	48	Moderate				
17		12:00 UTC 21 November 2013	36	Deep				
18		00:00 UTC 22 November 2013	24	Moderate				

Table 1 continued

Case no.	Storm name (feature)	Initial conditions	Forecast length (h)	Vortex depth	Remarks		
19	VSCS Lehar (Straight- moving)	00:00 UTC 25 November 2013	96	Moderate	A well-marked low pressure is seen on 21 November 2013 and concentrated into a depression over the south Andaman Sea. While moving northwestward, it intensified as a VSCS with a peak magnitude		
20		12:00 UTC 25 November 2013	84	Moderate	of ~ 75 knots. Later it rapidly weakened into a depression (45 knot change in 24 h; 00:00 UTC 27–28 November 2013). It made landfal over the Andhra Pradesh coast		
21		00:00 UTC 26 November 2013	72	Deep			
22		12:00 UTC 26 November 2013	60	Deep			
23		00:00 UTC 27 November 2013	48	Deep			
24		12:00 UTC 27 November 2013	36	Moderate			
25		00:00 UTC 28 November 2013	24	Moderate			
26	VSCS Madi (Recurved)	00:00 UTC 09 December 2013	96	Moderate	VSCS Madi is unique in terms of intensity and movement. It experienced re-curvature southwestward and weakened into a well-marked low pressure before making landfall over south Chennai, Tamil Nadu coast		
27		12:00 UTC 09 December 2013	84	Deep	F,,,		
28		00:00 UTC 10 December 2013	72	Deep			
29		12:00 UTC 10 December 2013	60	Deep			
30		00:00 UTC 11 December 2013	48	Deep			
31		12:00 UTC 11 December 2013	36	Moderate			
32		00:00 UTC 12 December 2013	24	Shallow			

respectively, which follow the TC vortex. The United States Geological Survey (USGS) data provided static land surface fields such as terrain/topography and land cover. The model physics included the simplified Arakawa–Schubert (SAS) scheme for cumulus parameterization and modified Ferrier cloud microphysics for explicit condensation. In the 3-km innermost domain of the model, only the microphysical parameterization explicitly resolved clouds.

The GFS planetary boundary layer parameterization was used. The GFDL scheme was used for surface flux calculations with an improved air—sea momentum flux parameterization in strong wind conditions and a one-layer slab land surface model. Radiation physics used the GFDL scheme. More details about the model can be found in Tallapragada et al. (2013), Osuri et al. (2017), and Nadimpalli et al. (2019). The analyses and 6-h forecast fields of GFS of the

National Centers for Environmental Prediction (NCEP) at $0.5^{\circ} \times 0.5^{\circ}$ horizontal resolution were used as the model's initial and boundary conditions.

2.1. Vortex Initialization and Relocation Technique

The purpose of VI is to improve the initial TC vortex for position, strength, and size. The three-dimensional structure of an initial vortex was modified in two ways: (1) size, in terms of the radius of maximum wind (RMW), the radius of 34-kt winds (R34), and radius of outermost closed isobar (ROCI), and (2) intensity, in terms of maximum sustained 10 m winds and minimum mean sea level pressure (MSLP). The observations/storm messages required to correct the initial TC vortex were obtained from "TCVitals" issued by IMD.

The HWRF VI process had three phases. First, a check was performed to access a preceding 6-h forecast if available. If this forecast was available and the initial intensity was greater than 14 m s⁻¹, it was considered a "cyclic-start" initialization; otherwise, it was a "cold start." A cyclic initialization went through the following three phases, while a cold start went through only phases 2 and 3:

Phase 1: Since the operational HWRF forecasts are run in cycles, a previous cycle 6-h HWRF forecast was separated into environment fields and a storm vortex.

Phase 2: The initial condition generated from GFS data was separated into environment fields and a TC vortex.

Phase 3: The TC vortex from the previous 6-h forecast (for cyclic initialization) or a bogus vortex (for cold initialization) was adjusted in its intensity and structure to match the observed TC center position, intensity, and structure information. The new vortex was merged with the GFS environment fields and relocated to the observed TC position, which was used to initialize both the outer and inner nested domains (D02 and D03).

More discussion on the cold and cyclic initialization in the HWRF system is summarized below.

Cold-start vortex initialization: When a previous cycle 6-h HWRF forecast vortex was not available (as was the case, for instance, for the first cycle of a TC),

a bogus axisymmetric vortex was used and adjusted as in phase 3.

Cyclic-start vortex initialization: A two-dimensional axisymmetric vortex created from the previous HWRF model forecast was used to generate the bogus vortex. The two-dimensional vortex was only required to be restructured once the model physics had undergone modification in the environment that strongly disturbed the storm structure. A forecast storm with a smaller R34 size, and a nearly axisymmetric structure was used to create the twodimensional vortex. The three-dimensional storm was separated from the storm's environmental field, and the two-dimensional axisymmetric part of the storm was calculated. The hurricane perturbations of horizontal wind components, specific humidity, temperature, and sea-level pressure were encompassed in the two-dimensional vortex. This two-dimensional vortex was used to generate the bogus storm. The two-dimensional vortex's wind profile was smoothed for creating the bogus storm until maximum wind speed or RMW was equal to the observed values. After that, the storm size and intensity were corrected. The same mechanism was followed for the vortex for the medium and deep-depth storms, while the shallow storms' vortex needs to go through two more final corrections: (i) the vortex top was set to 400 hPa, and (ii) the warm core structures were removed. More details have been provided in the supplementary text.

Stronger TCs are typically initialized by adjusting the TC vortex from the previous 6-h forecast. However, a bogus vortex can be used to initialize a stronger storm under the following four situations: (a) when the storm in the previous 6-h forecast was feebler than the observed intensity by > 50 knots, (b) the observed RMW was over 16 times bigger than during the last 6-h forecast, (c) the observed storm intensity was greater than 64 knots, and (d) the intensity correction factor (B) was more than 0.7. This procedure was different from what was done in previous HWRF implementations (Liu et al., 2013), in which a bogus vortex was used in all cold-start experiments. This change significantly improved the intensity forecasts in the first three cycles of a storm (Tallapragada et al., 2014).

A set of experiments was conducted using two strategies of VI methods. In the first experiment, a cold start was employed in each model initialization. In contrast, in the second one (known as cyclic start), the TC vortex was taken from the 6-h forecast of the previous forecast cycle of the HWRF model. Here onwards, cold start (cyclic start) will also be referred to as cold experiment (cyclic experiment). Note that the model's first forecast cycle was a cold experiment and not used in the analyses for a homogeneous comparison of cold-start and cyclic-start experiments. Note that no data assimilation was considered in these experiments, as the study's focus was to assess the capability of VI in improving the TC forecasting system.

The track forecasts were evaluated against best estimates of IMD with respect to the direct position error (DPE), longitudinal (zonal, or DX), and latitudinal (meridional, or DY) errors. The DPE is the great-circle distance between the model forecast position and the observed TC position at a particular forecast time. The cross-track (CT) and along-track (AT) errors determine the bias (left/right or ahead of/slower) in the model-forecasted TC position with respect to the IMD best track. Details on these positional errors are available in Fiorino et al. (1993) and Osuri et al. (2013).

3. Results and Discussion

The impact of the two different VI methods in simulation of the TC track and intensity for the different cases has been analyzed, and the results are presented here.

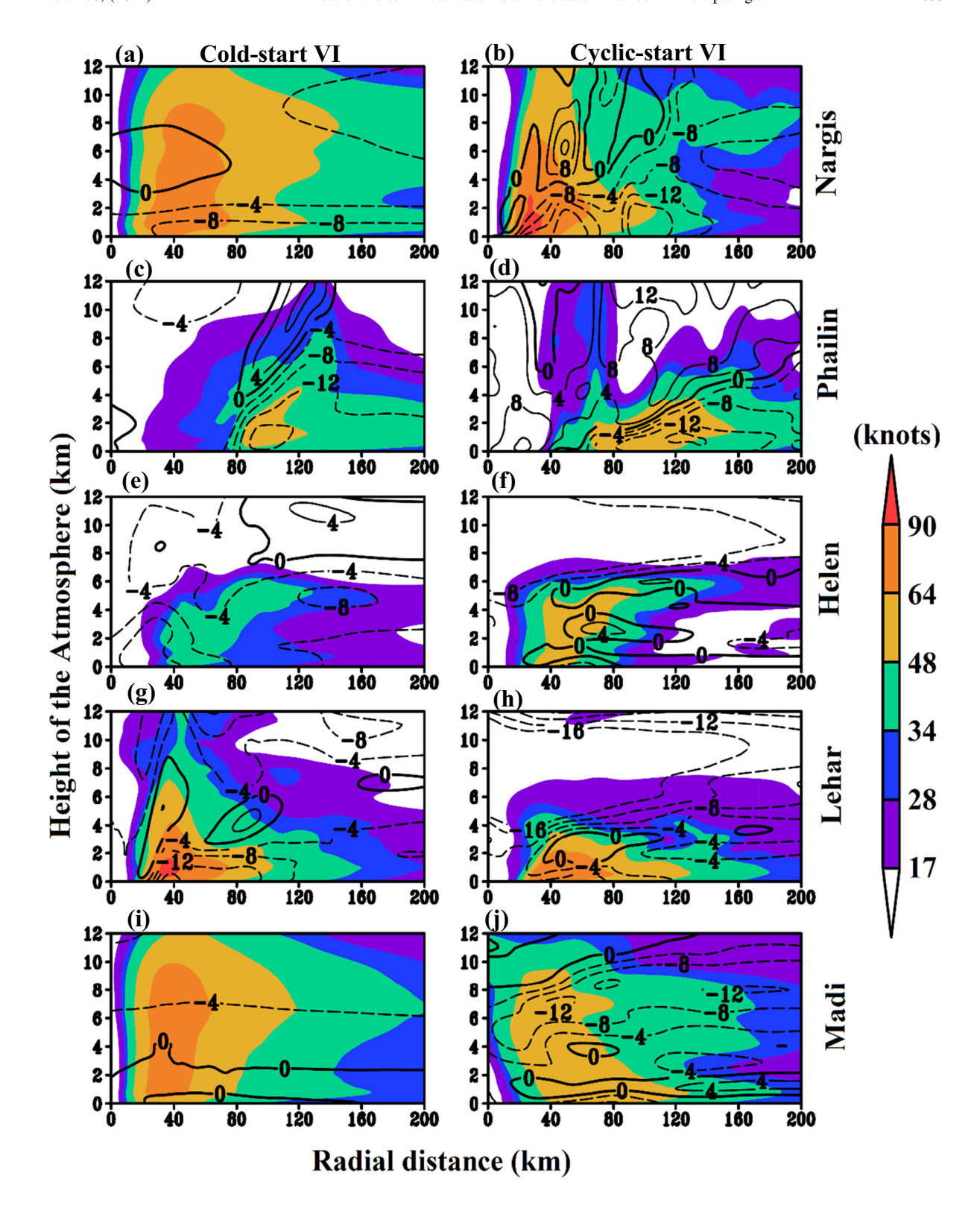
3.1. Improvement in the Initial Structures

The vertical structures of radial inflow (Vr) and tangential (Vt) winds of the initial vortex corrected by the two VI approaches are analyzed in Fig. 1. The results are for the representative cases (having a 72-h forecast lead from landfall) for the following TCs: Nargis (00:00 UTC 29 April 2008), Phailin (12:00 UTC 09 October 2013), Helen (00:00 UTC 20 November 2013), Lehar (00:00 UTC 26 November 2013), and Madi (12:00 UTC 09 December 2013).

Figure 1

Radial-height cross section of azimuthally averaged radial flow (contours, knot) and tangential wind (shaded, knot) at the initial time for TC Nargis from **a** cold-start VI, and **b** cyclic-start VI. **c-d**, **e-f**, **g-h**, and **i-j** are the same as **a-b** but for TCs Phailin, Helen, Lehar, and Madi, respectively

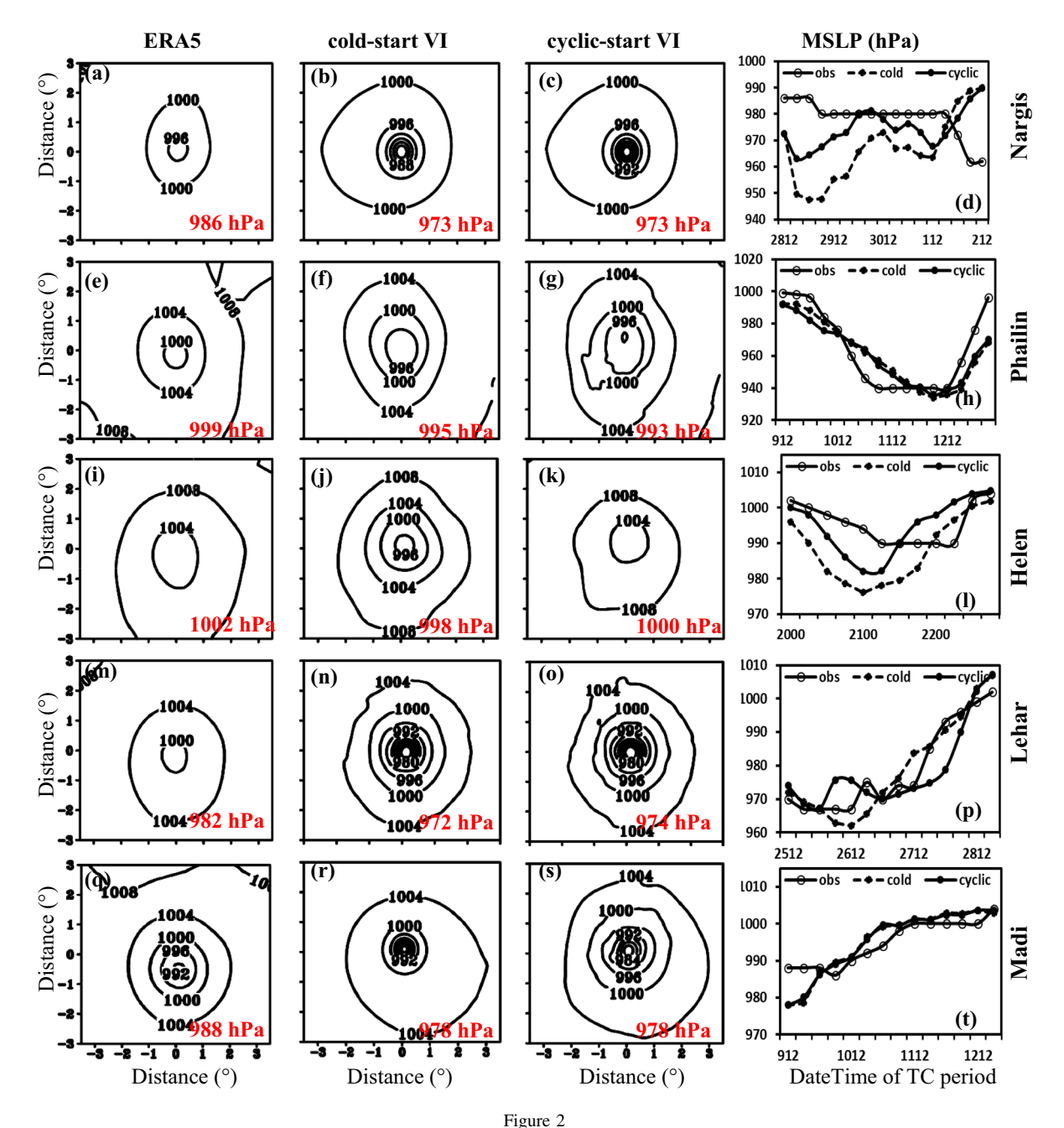
TC Nargis was a severe cyclonic storm (SCS; 48 knots < wind speed < 63 knots) of moderate depth (RSMC report, 2009). For Nargis, the azimuthally averaged Vt was stronger in the cyclic experiment vortex than in the cold one (< 90 knots). The inflow was weaker (about -8 knots) in the cold experiment (Fig. 1a), while it was more robust (greater than -16knots) up to a 120-km storm radius in the cyclic initialization (Fig. 1b). For TC Phailin, the initial vortex's height from the cyclic experiment (Fig. 1d) was comparable with that of the best estimates. The global storm message (TCVitals) showed a moderate vortex height at 12:00 UTC 09 October 2013 with cyclonic storm intensity (28-34 knots). The surface winds greater than 34 knots (cyclonic strength) were located 40 km away from the TC center in the cyclic experiment (Fig. 1d), while R34 was located 80 km away from the center in the cold experiment (Fig. 1c). The gradient in inflow near the TC center was high in the cyclic experiment vortex (Fig. 1c, d). For Helen, the inflow layer was deep in the cold experiment vortex. In contrast, the cyclic experiment vortex exhibited a shallow layer of inflow close to the surface and an outflow layer above it (Fig. 1e, f). For Lehar, the cold experiment exhibited a stronger Vt, more than 90 knots at the surface; however, the vortex's depth was not realistic. TC Lehar at 00:00 UTC 26 November 2013 was in the weakening phase (RSMC report, 2014), and the global analyses report that the depth of the vortex had been decreasing. The cyclic experiment vortex appeared to be decoupled with upper levels, resulting in a shallow vortex. The inflow in cyclic experiment vortex was weaker as compared to the cold experiment vortex (Fig. 1g, h). For Madi (12:00 UTC 09 December 2013), the cyclic experiment vortex was embedded with 48-64-knot wind, and its height was \sim 8 km (Fig. 1j). The cold experiment vortex was stronger (64-90 knots) and deeper (Fig. 1i). It was to be noted that the vortex of



the TC Madi was "deep" for most of the time until it crosses 15° N (where the weakening starts), except 12:00 UTC 09 December 2013. After that, the vortex of Madi was weakened into moderate and shallow for the subsequent initial conditions. Overall, results indicate significant changes in the inflow and the depth of the vortex between the cold experiment and cyclic experiment vortices. The cyclic experiment initialization has benefited from the incorporation of asymmetry in the initial vortex, which was expected to play an important role in intensity prediction.

The mean sea level pressure of the cases, as in Fig. 1, is shown in Fig. 2 from both the VI and ERA5 reanalysis. The time series of the forecasted MSLP from these experiments were also reviewed and compared with IMD best estimates. The minimum MSLP values for IMD best estimations (OBS) as well as for cold-start VI and cyclic-start VI experiments are shown in red in the corresponding subpanels. The main reason for considering ERA5 reanalysis data was its higher resolution (~ 31 km), reliability, and independence (Hodges et al., 2017). For Nargis, the cyclic- and cold-start VIs showed stronger vortex (973 hPa) in comparison to the ERA5 analysis (996 hPa) and IMD observation (986 hPa) at the initial time (Fig. 2a-c). Figure 2d shows the MSLP evolution indicating that the cold-start vortex deepened significantly during the integration, while the cyclic run improved the MSLP evolution, comparable to the observation. For Phailin, the cold- and cyclicstart initializations exhibited a similar MSLP structure. However, the cyclic vortex was slightly stronger with asymmetricity (Fig. 2e-g). Both runs could not capture a sudden pressure drop in the initial stage, which led to higher MSLP errors. However, both runs showed the maximum MSLP drop to 938 hPa and a sudden raising of pressure at the end (Fig. 2h). For Helen (Fig. 2i–l), the cyclic-vortex was more realistic than the cold one as seen from MSLP. The simulated weakening of Helen was early and large both in cyclic and cold experiments. However, Helen's weakening was described comparatively better in the cyclic run. In Lehar (Fig. 3m-p) and Madi's case (Fig. 3q-t), both the experiments showed similar MSLP evolution; however, the cyclic vortex was slightly weaker than the cold vortex in Madi. Upon comparing the initial MSLP of TC Madi from both the experiments against the IMD best estimations and ERA5 analysis, the weaker cyclic vortex is consistent.

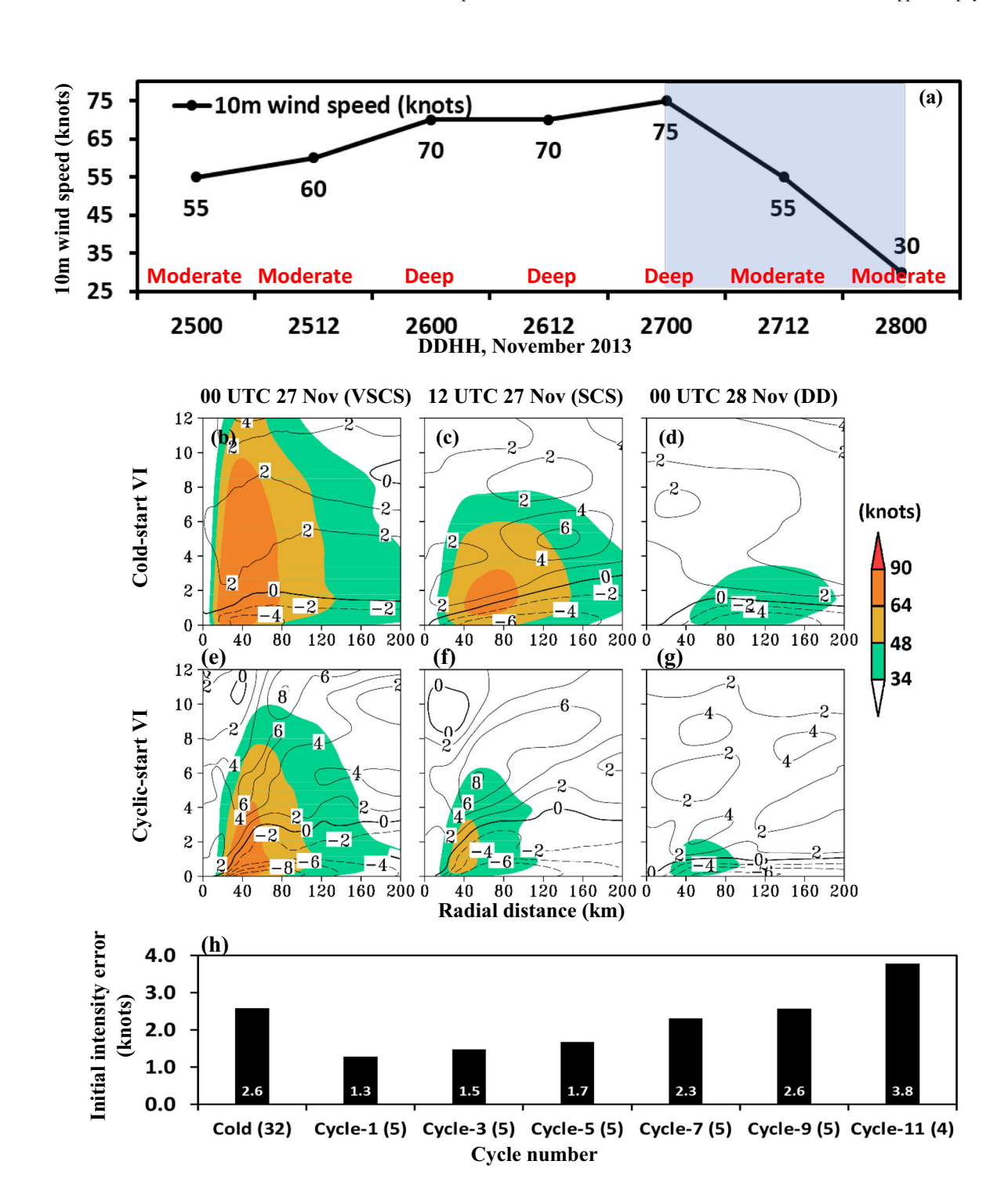
The cyclic experiment's positive impact in subsequent initializations was examined by considering the azimuthal average of radial-height structures of tangential wind (knots) and radial inflow at five initial conditions of VSCS Lehar in Fig. 3. Note that Lehar experienced a high-shear environment due to its relative proximity to the subtropical ridge and depth of the subtropical ridge (Bhalachandran et al., 2019). Thus, the onset of rapid decay (RD) in TC Lehar was notable from 00:00 UTC 27 November 2013 (wind strength was 75 knots) (Fig. 3a), and Lehar became a deep depression (DD) by 00:00 UTC 28 November 2013 with a surface maximum wind speed of 30 knots (45 knots change in 24-h duration). The initial vortex characteristics from 00:00 UTC 27 to 00:00 UTC of 28 November (corresponding to the RD phase) are shown in Fig. 3b-g. It was observed that the vortex strength and structure were almost similar in cold and cyclic starts when Lehar was in the intensification phase, i.e., up to 00:00 UTC of 27 November 2013. In the cold-start initialization, the initial vortex was deeper (9 km). The tangential wind magnitude was more than 64 knots at RD onset, corresponding to 00:00 UTC 27 November 2013 (where the system was at the VSCS stage). The inflow magnitude was about -4 to -6 knots in the boundary layer (Fig. 3b). Meanwhile, for the same time, the depth of the initial vortex with similar strength (> 64 knots) was confined to 4 km in the cyclic start, with a substantial inflow of ~ -8 knots in the lower atmosphere (Fig. 3e). The cyclic start could show the TC's weakening in the subsequent 12-h forecast, while the cold start maintained the intensity. At 12:00 UTC 27 November 2013, the tangential wind speed in the cyclic experiment was 34-63 knots, and the vortex height was 5-6 km (in terms of the vertical extent of 34-knot wind contour). The cold-start vortex was extended up to 7 km and was stronger (tangential winds were 64-90 knots). Both the vortices exhibited a notable change in size (horizontal extent of 34-knot wind contour). TC Lehar was bigger (~ 200 km) in the cold-start run (Fig. 3c), while the cyclic vortex size was confined within 100 km (Fig. 3f). After Lehar attained the deep depression (DD) stage at



Mean sea level pressure (MSLP, hPa) contours for TC Nargis from a ERA5 analysis, b cold-start VI, c cyclic-start VI, and d time series of MSLP simulated from experiments and IMD best estimate. e-h, i-l, m-p, and q-t are the same as a-d but for TCs Phailin, Helen, Lehar, and Madi, respectively. The red-colored numbers are the minimum value of MSLP from OBS, cold start, and cyclic starts, as mentioned in corresponding subpanels. The axes in the first three columns indicates the distance (in °) from the TC center (zero in the axes)

00:00 UTC 28 November 2013, 34-knot winds in the cold start were spread between 40 and 180 km from the TC center and vertically extended up to 2 km

from the surface. Unlike the cold start, the cyclic vortex was comparatively weaker (34 knots) with a horizontal spread between 30 and 90 km from the



▼Figure 3

a 10 m wind speed of TC Lehar from IMD best estimation. Heightzonal cross section of initial wind structures (knot) for TC Lehar from cold-start VI experiments (b-d), and cyclic-start VI experiment (e-g) for different initial conditions. h Stratification of mean initial intensity error with respect to number of continuous forecast cycles (after first cold start). The number of cases considered in the mean is mentioned in the parenthesis of the x-axis of (h). "Moderate" and "deep" in (a) represent the depth of the vortex at the corresponding time mentioned in the x-axis

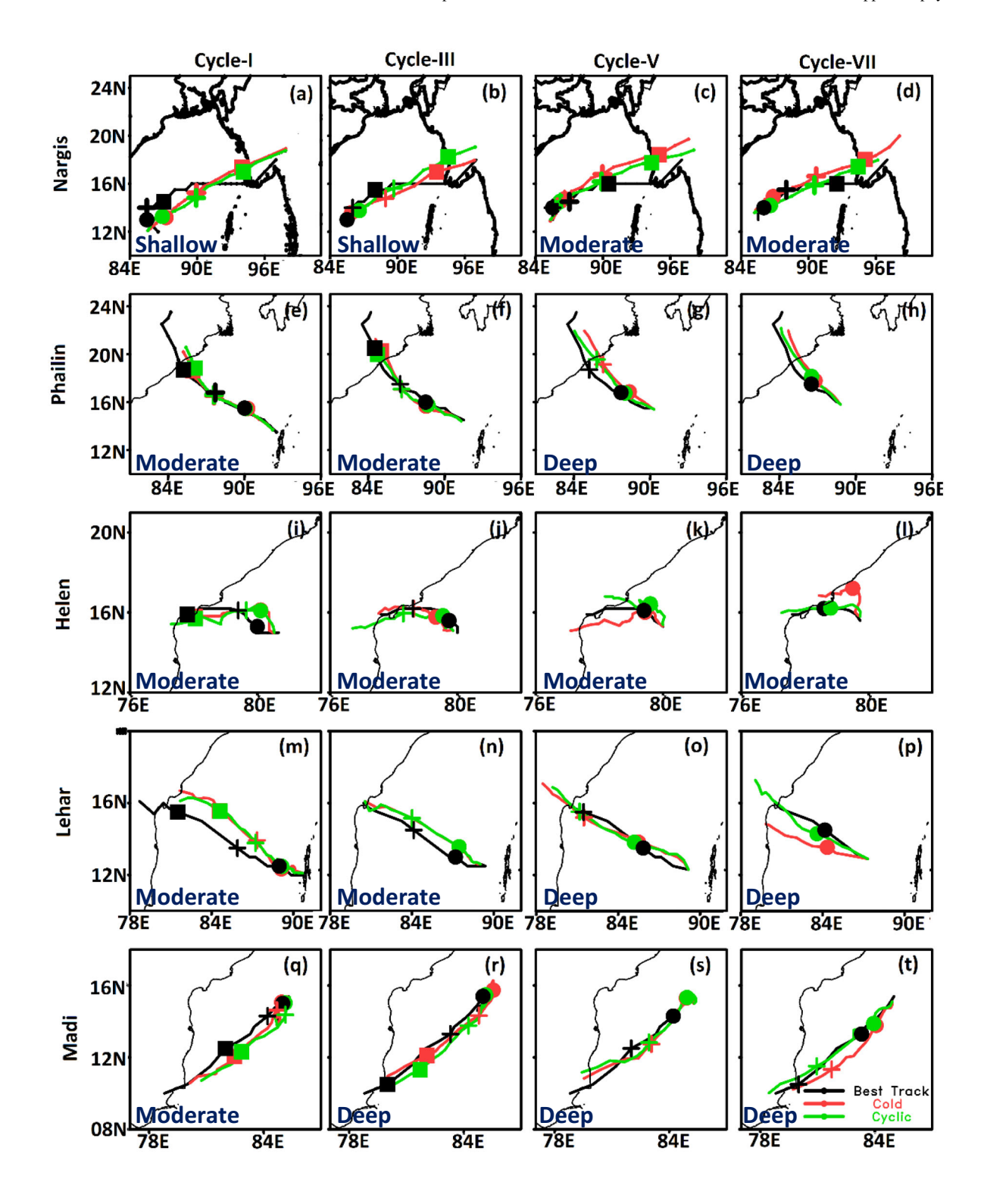
storm center. The larger TC size in cold-start initialization could result from the higher intensity of Lehar (Wu et al., 2015). This (Fig. 3b–g) gives a sequence of the RD from cyclic experiments and correlates with the intensity decay.

Figure 3h shows the average error of 10 m wind (knots) for different cyclic-start initialization numbers. The first through the ninth cyclic initializations are referred to as the cycle 1 through cycle 9, respectively. On average, the cyclic-experiment VI showed lesser errors up to cycle number 7 (cycle 7). Beyond cycle 9, the cyclic experiment resulted in higher errors than cold-experiment initializations.

The storm-based mass-weighted deep-layer mean wind magnitude and direction at the initial time (t = 0), averaged over a radius of 600 km from the TC center for each TC case, was also computed. A recent study demonstrated the positive impact of the cyclic initialization on TC environmental flow and storm-scale wind asymmetry associated with the TC (refer to Figs. 2, 3, and 4 of Osuri et al., 2017). The mean error between the model result and satellite analysis (available from http://rammb.cira.colostate. edu/products/tc realtime) in direction and magnitude was found to be 45 degrees and 12 knots, respectively, for the cold experiments. In contrast, the cyclic experiment yielded corresponding errors of 35 degrees and 5 knots. The individual case analysis showed higher errors in the direction (~ 50 degrees) for sudden recurving cases (TC Madi), and the cyclic experiments captured features with smaller errors (\sim 36 degrees) as compared to the satellite-derived direction. The correct representation of the wind flow at the initial time could be one of the reasons for better predictions from cyclic experiments. Individual analyses of each TC case indicate that the steering strength was stronger (overestimated) in the Nargis case for cyclic experiments.

3.2. Mean Track Forecast Errors

The HWRF model-predicted tracks from both cold-start VI and cyclic-start VI experiments along with IMD best track estimations are shown in Fig. 4 for different cycles of TCs analyzed in this study. Overall, the results indicated that when the TC was initiated with a shallow vortex, the track prediction was nearly the same for both experiments. Table 2 shows the mean track errors in terms of DPE, CT, and AT errors from both experiments. Recent studies have found mean track errors of operational forecast (Mohapatra et al., 2013a, 2013b) and the highresolution Weather Research and Forecasting (WRF) model (Osuri et al., 2013) over the NIO basin. The prediction skill (%) of cold-start VI and cyclic-start VI experiments was calculated against the operational errors provided in Mohapatra et al. (2013a) and WRF model errors from Osuri et al. (2013) as base values. The positive (negative) values of gain in skill (%) represent the gain (loss). The performance evaluation against Mohapatra et al. (operational errors) and Osuri et al. (model errors) can provide sufficient confidence for TC consensus forecast for the basin. From Fig. 5a and b, the skill was considerably higher for the cyclic experiment than for the cold experiment up to 36-h forecast. The cyclic experiments also showed a diminution of improvement in skill compared to cold experiments for 72 h. The gain in skill varied from 15 to 83% for the cold experiments, while cyclic experiments showed the skill in the range of 26–78% for 12–72-h forecasts. The HWRF model's skill was better than that of the WRF (Osuri et al., 2013), and it could be because Osuri et al. (2013) used a coarser (9-km) horizontal resolution. The gains in skill (%) from the cold experiments over Osuri et al. (2013) were 41%, 27%, 26%, 62%, 68%, and 80% for 12, 24, 36, 48, 60, and 72 h, respectively, while the cyclic experiments show superior performance by 49%, 48%, 43%, 61%, 73%, and 74% for 12, 24, 36, 48, 60, and 72 h, respectively. This result primarily highlighted that higher resolution improved the model skill. The gain in skill (%) of cyclic experiments over cold experiments was



▼Figure 4

Model-simulated tracks from cold-start VI (red) and cyclic-start VI (green) along with IMD best track estimations (black) for TC Nargis from a cycle 1, b cycle 3, c cycle 5, and d cycle 7. e-h, i-l, m-p, and q-t are the same as a-d but for TC Phailin, TC Helen, TC Lehar, and TC Madi. Refer to Table 1 for the time of initialization. The dot, cross, and square in each figure mark the 24-, 48-, and 72-h observed/simulated position. The corresponding depth of the vortex at the initialization time of each run is indicated as "Moderate" or "Deep" in the bottom of each subpanel

also calculated and given in Table 2. The cyclic experiment exhibited higher skill for the 24-h forecast (by 29%) and was comparable to the cold experiment for the 48-h forecast (skill is -3%). In comparison, the cold experiment was better than the cyclic experiment for the 72-h forecast (by 28%). The vortex initialization scheme could generate the vortex over the open waters with no data or very little data near the TC. Note that the bogus vortex (in cold starts) lacked the asymmetry in the wind circulation. The spin-up vortex in the cyclic start could provide the asymmetry to the wind circulation (Das et al., 2015; Osuri et al., 2017; cross-references), and the VI corrected the TC position, circulation, and strength based on TCVitals (Liu et al., 2020; Tallapragada et al. 2014). Further, Liu et al. (2020) and Tallapragada et al. (2014) concluded that the first 1-3 cyclic starts significantly improved the track over cold starts. The possible reasons for improved track predictions were (i) storm size corrections (Liu et al., 2020) and (ii) improved large-scale circulations and low-level asymmetric wind flows in the vicinity of TC centers when initializing the vortex in cyclic mode at high resolution (Wu et al., 2015; Osuri et al., 2017).

It is worth noting that the DPEs of the cyclic experiments were comparable with those of cold experiments at times. Individual case analyses indicated that the HWRF model failed in capturing the track of Nargis, particularly the eastward movement (00:00 UTC 01 May 2008 to 15:00 UTC 02 May 2008). During the same period, the simulated TC moved northeastward. This deviation caused the simulated TC to cross the Myanmar coast much earlier than the actual. This led to higher DPE errors in cold-start VI and cyclic-start VI experiments. The mean DPEs excluding the Nargis case indicated that the cyclic run showed better performance than the cold run up to 36-h forecast length. Suppose Nargis was excluded from the mean error computation. In that case, the short-range prediction errors decreased to 36, 45, and 55 km for 12-, 24-, and 36-h forecast lengths from cold experiments, while the same for the cyclic run were 26, 40, and 41 km, respectively. Analyzing an individual TC case from the experiments, the mean error of TC Nargis from initial condition at 12:00 UTC 27 April 2008 and 00:00 UTC 28 April 2008 ranged from 70 to 350 km for 6-96-h forecast lead times (refer to Fig. 4a and b), which contributed to higher mean errors.

To understand the model behavior in simulating the movement of the TCs, the simple mean of CT and AT errors were calculated (not shown). The CT and

Table 2

Mean direct position error (DPE, km), absolute cross-track (CT, km) error, and absolute along-track (AT, km) error of the predicted TC tracks from cold-start VI and cyclic-start VI experiments up to 72-h forecast length for NIO TCs

Forecast length in	Direct position error		Absolute cross-track error		Absolute along-track errors		% of improvement in DPE over cold experiments
hour (no. of cases)	Cold Cyclic		Cold Cyclic		Cold Cyclic		
12 (32 cases)	61 (16)	53 (13)	11 (36)	2 (25)	93 (40)	75 (45)	13
24 (32 cases)	84 (28)	60 (16)	0 (40)	46 (43)	64 (38)	60 (26)	29
36 (28 cases)	104 (34)	81 (16)	32 (44)	11 (35)	93 (54)	121 (64)	22
48 (24 cases)	77 (39)	79 (29)	22 (38)	7 (49)	129 (82)	69 (77)	-3
60 (20 cases)	89 (49)	73 (30)	27 (90)	41 (80)	72 (43)	98 (59)	18
72 (16 cases)	67 (56)	86 (40)	70 (0)	36 (33)	107 (102)	4 (26)	-28

95% confidence interval (CI) is shown in parenthesis. [Bold indicates relatively better performance between the cold versus cyclic experimental run]

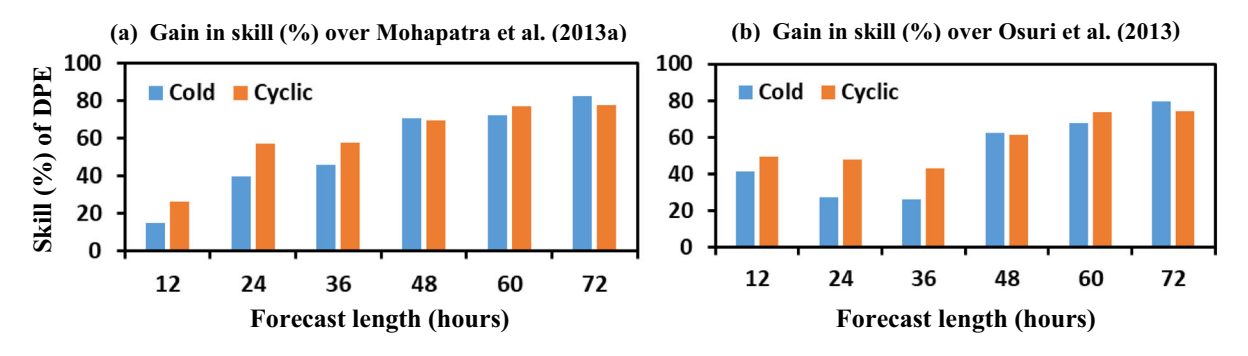


Figure 5
Gain in skill (%) of cold-start VI and cyclic-start VI experiments for mean DPE computed against **a** operational errors reported in Mohapatra et al. (2013a) and **b** WRF model errors of Osuri et al. (2013)

AT errors are negative for all the forecast lengths. Negative CT errors indicated the leftward bias, while the negative AT errors indicated the slower movement of TC in the HWRF simulations. The results were consistent with those reported for the Atlantic and Pacific basins by Tallapragada et al. (2015). However, the CT and AT errors are relatively less in the cyclic-start VI experiment. To quantify the errors, the mean absolute CT and AT errors (Table 2) indicated that the cyclic experiment was comparable or superior to that of the cold-start VI experiment at most forecast lengths. At longer forecast times (except at 60-h forecast), CT error magnitude was more in the cold-start VI experiments (22-70 km in 36–72-h forecast length) compared to cyclic-start VI experiments (7-41 km in 36-72-h forecast length). The mean absolute AT errors (Table 2) indicated that the cyclic experiment was comparatively better than the cold run for most forecast lengths. Analysis of individual cases revealed that Nargis' mean CT errors ranged from 28 to 500 km, indicating the right deviation from the observed track. Negative AT errors of Nargis ranging from -37 to -685 km highlighted slower movement than the observed translation speed. The overall gain in skill (%) of the model experiments for CT and AT errors over long-term averaged errors from Osuri et al. (2013) were also computed (not shown). The CT errors showed notable improvements of $\sim 24\%$ and \sim 56% skill from cold- and cyclic-start VI, respectively. Thus, the results indicated that the HWRF could provide better guidance on the area of evacuation and timing of landfall compared to the WRF model.

3.3. Mean Intensity Errors

The 10 m maximum sustained wind speeds (knots) from three representative cases, VSCS Phailin (12:00 UTC 09 October 2013), VSCS Lehar (00:00 UTC 26 November 2013), and SCS Helen (00:00 UTC 20 November 2013), are shown in Fig. 6a-c. These three TCs are unique in the intensification process. The VSCS Phailin exhibited rapid intensification (RI) (Mohanty et al., 2015; Osuri et al., 2017). The VSCS Lehar has rapidly weakened before the landfall (Bhalachandran et al., 2019), while SCS Helen showed "normal" intensification. The cyclic experiment could capture the rapid increase in intensity for 12-36-h duration (in Fig. 6a) and rapid weakening for a 24-48-h duration (in Fig. 6b), close to observation. The cold experiment did not show such rapid intensity changes during the same period. However, it could capture the maximum or minimum intensity magnitudes of the TC Phailin and Lehar. In the first 24-h forecast of Lehar (Fig. 6b), the intensity evolution was almost similar in both the experiments. After the onset of rapid decay at 24-h forecast length, the cyclic experiment could pick up the realistic intensity decrease. The cold experiment captured the trend, but showed a large positive bias. In the case of Helen, both the experiments exhibited higher intensity over IMD best estimates. However, the cyclic experiment showed lesser biases compared to the cold experiments (Fig. 6c). Similar results have been observed in other cases.

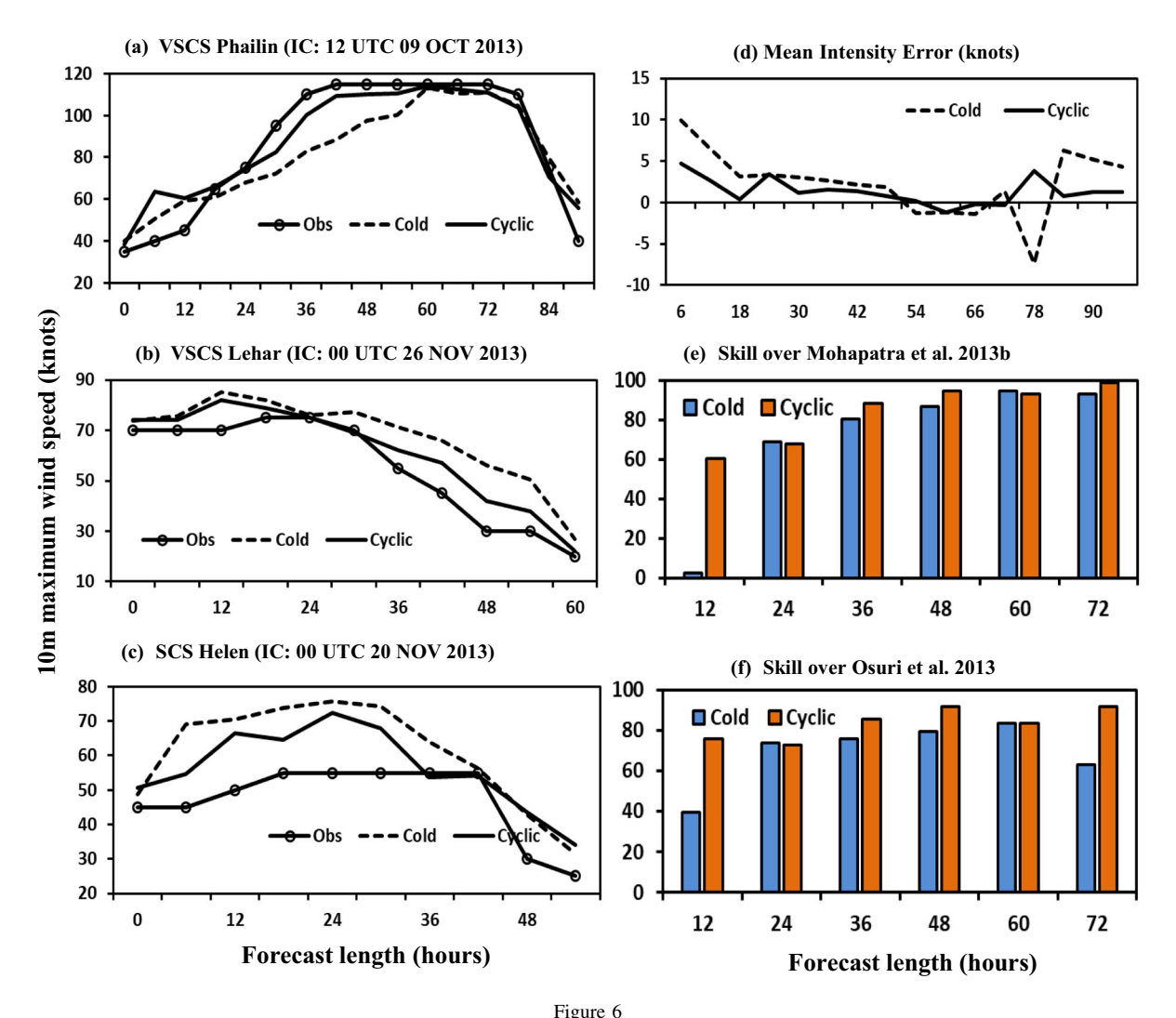
Figure 6d shows the mean forecast error of 10 m wind speed (knots) from all 32 cases. The cyclic experiment was superior in the first 18-h forecast of intensity, limiting the error to < 5 knots. The cold run showed maximum error in the 6-h forecast due to a bogus vortex initialization. The mean errors were almost similar for both the experiments from 24- to 72-h forecast. After the 72-h forecast, the cyclic experiments showed fewer errors than the cold run. The correct representation of the wind flow at the initial time also could be one of the reasons for better predictions from cyclic runs (Osuri et al., 2017). The gains in skill (%) in mean intensity error over Mohapatra et al. (2013b) and Osuri et al. (2013) were computed and shown in Fig. 6e and f, respectively. The skill of the cold run was almost the same as that of the operational 12-h forecast, while the cyclic run was more skillful (61%). This highlights the need for cyclic vortex initialization in the operational TC forecast. In the 24-h forecast, both cold-start and cyclic-start VI experiments exhibited similar skills (68%). As the forecast length increased, the HWRF model's skill increased from both cold and cyclic VI experiments. The gain in the skill of the cold- and cyclic-start VI experiments over the operational forecast was 87% and 95%, and 93% and 99% for 48 and 72 h, respectively (Fig. 6e). The skill of cold and cyclic runs followed a similar trend as that noted against the operational forecast. The gain in the skill of the HWRF over the WRF forecast was also considerably high (Fig. 6f). Overall analyses of track and intensity forecast errors of the HWRF model indicated that the HWRF forecast was superior for intensity and track forecast as compared to the operational forecast and WRF model.

3.4. Mean Forecast Errors w.r.t. Intensity at TC Initialization

By considering the TC forecasts initialized at various intensity stages such as depression/deep depression (D/DD), cyclonic storm (CS), severe cyclonic storm (SCS), and very severe cyclonic storm (VSCS), the performance of the cold- and cyclic-start VI experiments for track prediction was

evaluated. Figure 7 shows the mean of the DPE, CT, AT, and intensity errors for different forecast lengths. At the D/DD stage, only cold experiments were carried out because of the method followed (shallow vortex) in VI. Hence, similar errors were observed in both the experiments (Fig. 7a). Both the experiments at CS stage initializations also exhibited similar DPEs (Fig. 7b). In some CS initializations, the cyclic VI also produced symmetric vortex similar to the bogus vortex; thus, the DPEs in cold- and cyclic-start VI runs were nearly the same (not shown). The DPE (Fig. 7c, d) was significantly less in cyclic experiments when the model was initialized at higher intensities (SCS and above intensity stages). There was an improvement of 30% and 45% for the cases initialized at the SCS and VSCS stage. Especially for higher forecast lengths (> 60 h), there was a significant improvement ($\sim 85\%$) in the track prediction (Fig. 7c, d). Moreover, the cyclic experiment exhibited consistent errors with a smaller confidence interval (CI) at 95% confidence. This improvement in the prediction was mainly due to the improved symmetric representation of the vortex in the cyclic experiment and treatment of vortex height and its correction (Tallapragada et al. 2014; Osuri et al., 2017).

The CT errors (Fig. 7e-h) in cold-start and cyclicstart VI experiments were relatively small, but the AT errors (Fig. 7i-1) were high. The cyclic experiment performed better in terms of AT errors with a smaller CI (at 95%) than those from the cold experiments. The results demonstrated that the "stronger" the storm, the lesser the track forecast error range. Furthermore, the mean intensity errors of the TC stage (Fig. 7m-p) also followed a similar pattern as DPE for weaker TCs (such as DD or CS stage). Once the system attained SCS (and above) intensity, the mean errors were reduced significantly in the cold experiment's cyclic predictions. The mean intensity errors from cyclic experiments were 3, 8, and 4 knots for 24-, 48-, and 72-h forecast lead times, respectively. In contrast, the cold experiment exhibited 5, 10, and 12 knots for the same forecast leads. When comparing the cold-start and cyclic-start VI experiments, the track was comparable for weaker-intensity initializations. However, the cyclic vortex initialization was superior for intensity prediction most of the



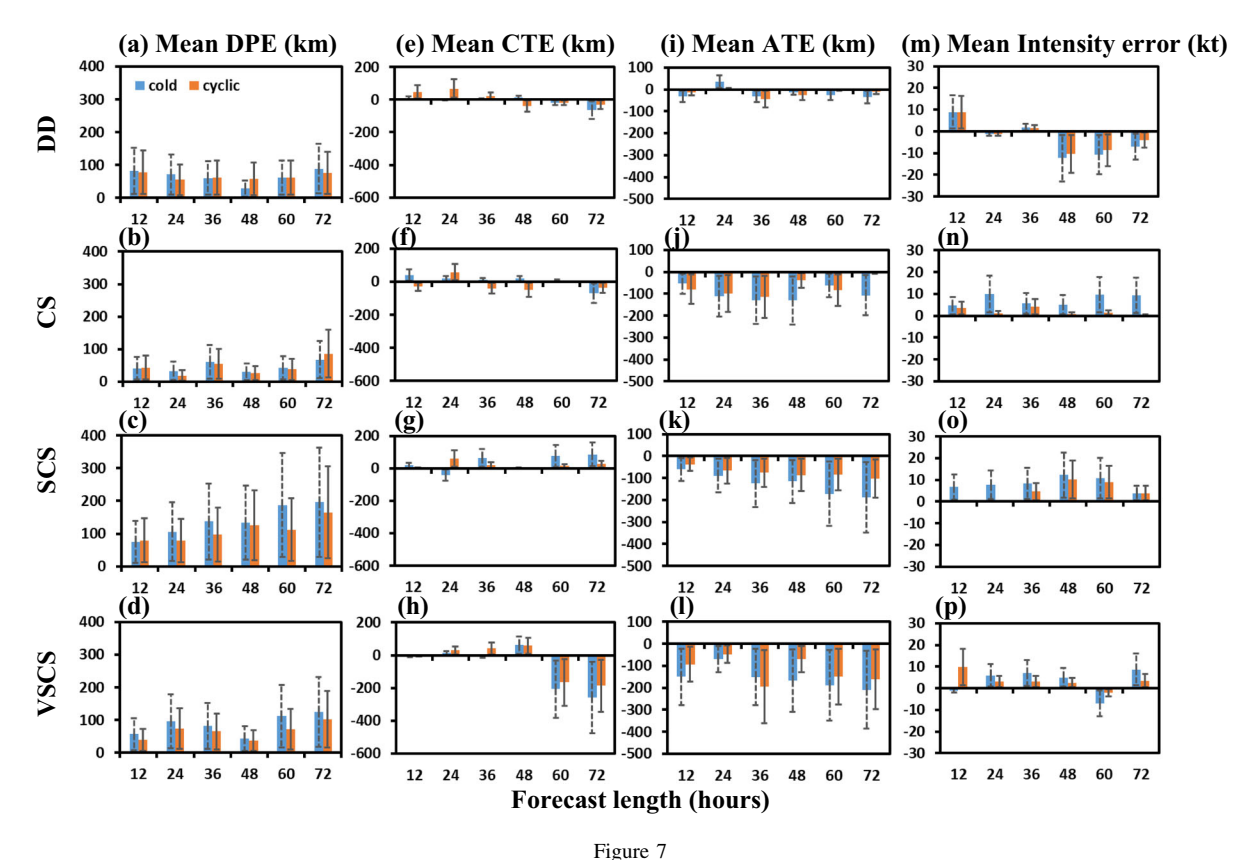
Evolution of **a** 10 m wind speed (knots) of VSCS Phailin (IC: 12:00 UTC 09 October 2013) from cold-start and cyclic-start VI experiments along with IMD best estimates. **b** and **c** are the same as **a** but for VSCS Lehar (IC: 00:00 UTC 26 November 2013) and SCS Helen (IC: 00:00 UTC 20 November 2013). **d** Mean intensity error (knots) for cold- and cyclic-start VI experiments from all cases. **e** Gain in skill (%) of intensity prediction over operational forecast errors reported in Mohapatra et al. (2013b) and **f** of WRF model forecast from Osuri et al. (2013)

time. Further, the 95% CI was also less, indicating higher consistency (less error spread).

3.5. Model Diagnostic Analysis

TCs Phailin and Lehar exhibited RI and rapid weakening, respectively (Fig. 6a, b). TC Helen represented a typical intensified system, and both the cold-start and cyclic-start runs did well in predicting the intensity. As shown in Fig. 6a, b, the cold and cyclic runs exhibited considerable intensity

changes in their forecast. Hence, Phailin and Lehar have been considered representative cases for understanding the processes leading to different intensity rates in the cold-start and cyclic-start runs. Many factors control the development and intensification of a TC, one of which is the availability of dry air in the storm's vicinity. Dry air may prevent ascending air parcels from reaching saturation, decreasing net condensation and latent heat release. The time/height cross sections of the $(3^{\circ} \times 3^{\circ})$ domain-averaged equivalent potential temperature $(\theta_{\rm e})$ were compared



Mean track error (km) and 95% confidence intervals of cold-start VI and cyclic-start VI experiments when the vortex initialization is at **a** DD, **b** CS, **c** SCS, and **d** VSCS stages. (**e-h**), (**i-l**), and (**m-p**) are the same as (**a-d**) but for mean CT error (km), mean AT error (km), and mean intensity error (knots) of both the experiments, respectively. Y-axis indicates the error (in km)

for TC Phailin (initialized at 00:00 UTC 26 November 2013) and TC Lehar (initialized at 00:00 UTC 26 November 2013) from both the experiments in Fig. 8a-d. Bhalachandran et al. (2019) explained the role of θ_e in providing the thermodynamic mechanism for the intensification of these TCs. The time evaluation of θ_e provided an evident relation between the vertical wind shear and the ventilation of environmental dry/cold air into the mid-levels of a TC. A steady, moderate-high value of θ_e was seen in TC Phailin with little to no apparent gradient until its landfall in both experiments. For TC Phailin, the $\theta_{\rm e}$ modified rapidly due to persistent and deep convection from the surface, and led to sustained maximum winds until landfall (Fig. 8a, b). Figure 8c and d shows a clear correlation of vertical wind and ventilation effect (intrusion of dry air) for TC Lehar from cyclic experiments (Fig. 8d). The overlay of domain-averaged vertical winds also showed weaker updrafts (< 0.3 m/s) from the cyclic experiment for TC Lehar. In contrast, the cold experiment showed stronger updrafts and large moisture availability (θ_e) in the mid-levels that sustained the storm intensity in this simulation. According to Tang and Emmanuel (2010), a decrease in the azimuthal mean θ_e was associated with reducing the Carnot engine's thermodynamic efficacy.

Since, in the cold experiments of TC Lehar, θ_e was more abundant in the middle layers (Fig. 8c), the vertical wind extending upward from the surface signified the upward transport of moisture. A quadrant-averaged vertical velocity (w) and θ_e were also computed (not shown) to understand the asymmetric distribution of θ_e in the experiment of the intensification/weakening process. Positive vertical velocities indicated that the convective updrafts are present in

each of the four quadrants in the eyewall region. In TC Lehar's case, a sharp gap in the near-surface $\theta_{\rm e}$ gradient was responsible for the onset weakening in the cyclic experiment. The result showed that higher moisture was initiated by horizontal moisture flux convergence and transported the moisture vertically upward that provided a favorable environment for more vigorous and sustained convection and latent heat release that resulted in RI of TC Phailin.

Previous studies demonstrated the close relationship between the cloud condensate and release of latent heat with the TC intensity and intensity changes (Hack & Schubert, 1986; Nolan et al., 2007, 2019). Thus, an analysis was undertaken to understand the characteristic changes in the cloud

condensate corresponding to Phailin and Lehar's intensity evolution. Figure 9a–d shows the time/height evaluation of total condensate averaged over the 3° × 3° domain for VSCS Phailin (initialized at 00:00 UTC 26 November 2013) and Lehar (initialized at 00:00 UTC 26 November 2013) from both the experiments. The higher cloud condensate resulted in higher water quantity detrained from deep convection to a large scale and intensity (Storer et al., 2015). The mean divergence (convergence) was plotted in a contour overlay. In the case of Phailin (Fig. 9a, b), the higher cloud condensate amounts were formed in 500–300 hPa layers. In both the experiments (cold and cyclic VI), higher condensate and surface convergence were simulated. However, the cyclic

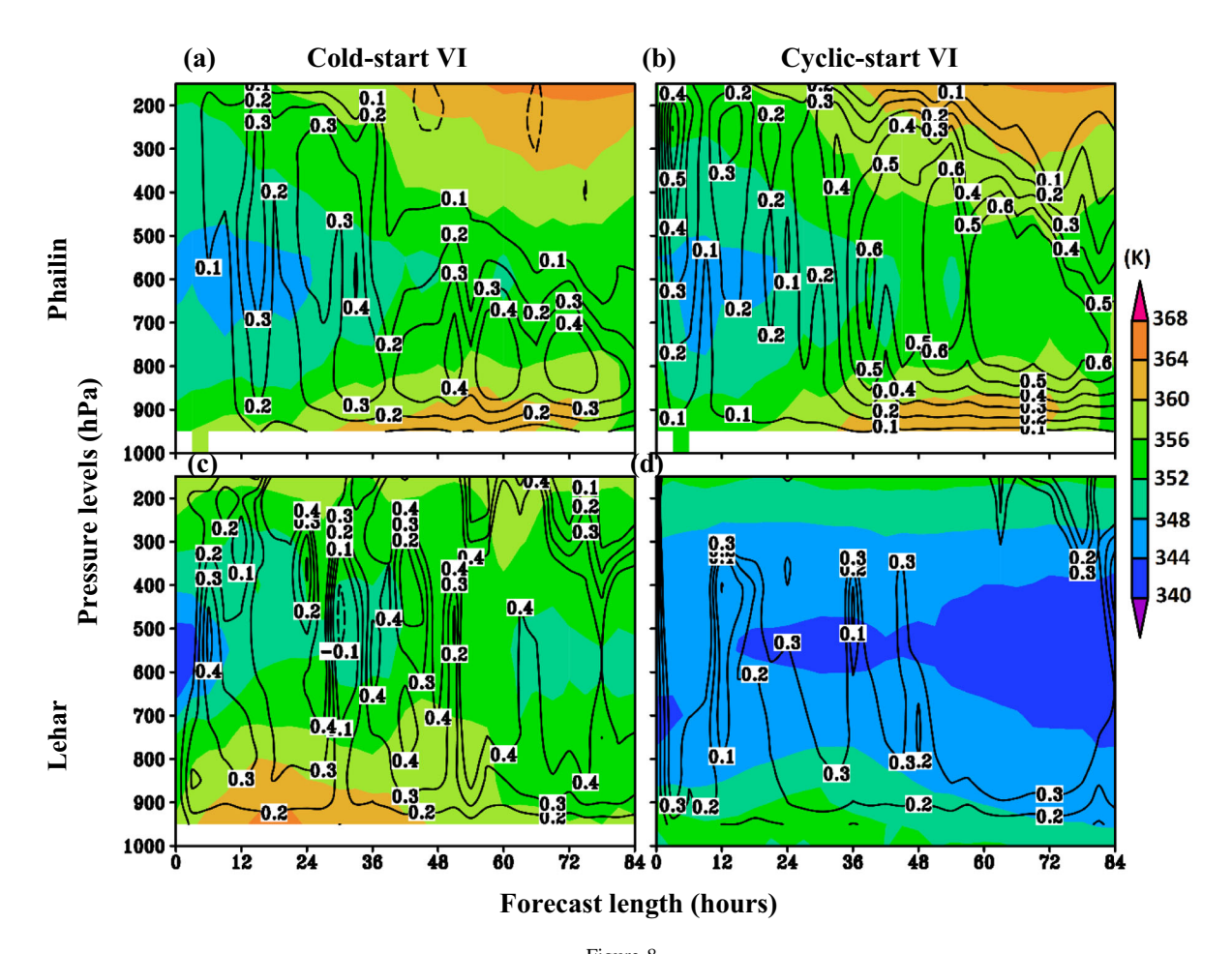


Figure 8

Time/height cross section of domain-averaged equivalent potential temperature (θ_e in K) and vertical velocities (m s⁻¹) for VSCS Phailin from both **a** cold-start VI and **b** cyclic-start VI experiments initialized at 12:00 UTC 9 October 2013. **c**, **d** are the same as **a**, **b** but for VSCS Lehar initialized at 00:00 UTC 26 November 2013. The fields are averaged over a domain of $3^{\circ} \times 3^{\circ}$ around the TC center

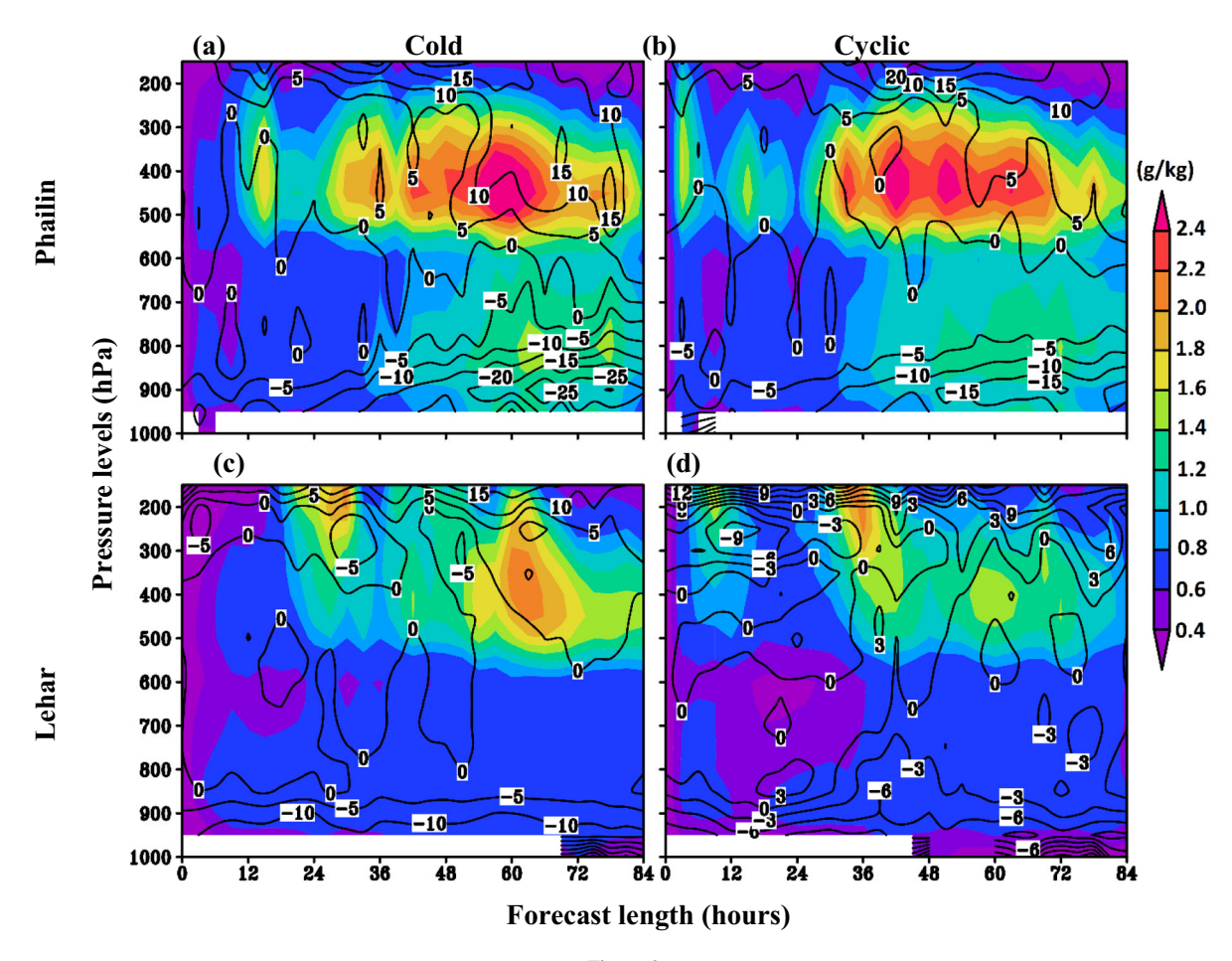


Figure 9

Time/height evolution of averaged total condensate (g kg⁻¹, shaded) and divergence/convergence (s⁻¹, contours) over a storm radius of 100 km from VSCS Phailin's center from **a** cold-start VI and **b** cyclic-start VI experiments initialized at 12:00 UTC 9 October 2013. **c**, **d** are the same as **a**, **b** but for VSCS Lehar initialized at 00:00 UTC 26 November 2013. Note that the positive and negative contours represent convergence and divergence, respectively

experiment (Fig. 9b) captured more elevated amounts (> 2.2 g kg⁻¹) from the 24-h forecast onward. The convergence induces radial inflow in the lower troposphere, which in turn transports moisture radially inward. Figure 9c-d shows that the lesser amounts of cloud condensate were formed in the cyclic experiment (Fig. 9d) for VSCS Lehar. A dry slot was seen in the cyclic start experiment during 12–36 h in the mid-levels of Lehar (Fig. 9d), unlike in cold start experiments (Fig. 9c). For the cold experiment, higher amounts of cloud condensates and higher surface convergence were simulated. The radial distribution of cloud condensate (not shown) for TC Lehar at different stages was also correlated

with the rate of change (rapid fall) in 10 m winds (Fig. 6b). The cloud condensate was likely influenced by the cycled fields of surface winds (convergence/divergence), temperature, and moisture (as θ_e and release of latent heating).

To further confirm moisture's role in the rapid intensification (weakening) of VSCS Phailin (Lehar), the Hovmöller diagram of columnar-averaged vertical mass flux within a 100-km radius from the TC center was computed and shown in Fig. 10a and c. The tangential wind (V_t) was also analyzed (Fig. 10b and d), which correlated with the columnar vertical mass flux rate for VSCS Phailin and VSCS Lehar. It was clear from the results that TC Phailin exhibited a

4068 R. Nadimpalli et al. Pure Appl. Geophys.

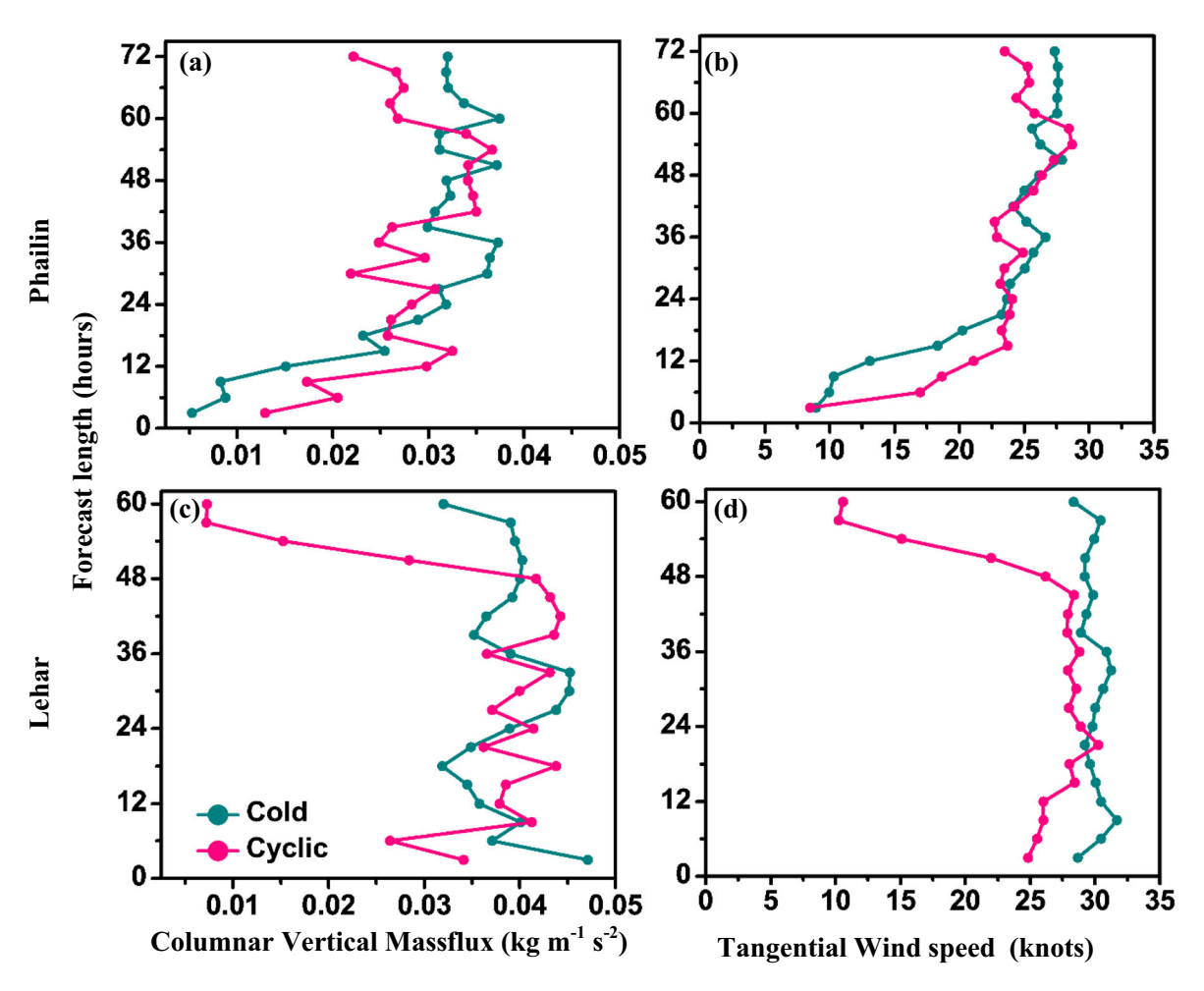


Figure 10
Temporal evolution of columnar-averaged **a** vertical mass flux (kg m⁻¹ s⁻²) and **b** tangential wind (knots) over a storm radius of 100 km from VSCS's Phailin center from cold-start VI and cyclic-start VI experiments initialized at 12:00 UTC 9 October 2013. **c**, **d** are the same as (**a**, **b**) but for VSCS Lehar initialized at 00:00 UTC 26 November 2013. Note that the Y-axis is forecast length (**h**) in these figures

similar pattern for vertical mass flux (Fig. 10a) and the tangential wind speed (Fig. 10b). As stated, VSCS Phailin was one of the strongest cyclones among all TCs occurring over the BoB. TC Phailin had a moisture-rich environment and an intense vortex TC. In the case of Lehar, a sharp drop after 48 h was observed in mass flux (Fig. 10c), along with a rapid reduction in the tangential winds from the cyclic experiment. The cold experiment did not produce the same. These results reaffirmed that the HWRF model when operated with cyclic-start mode improved the simulation of the TCs over the BoB basin.

4. Conclusions

This study examined the impact of two different (cold-start and cyclic-start) vortex initialization and relocation techniques in the HWRF system for TC prediction over the Bay of Bengal based on 32 forecast cases of five recent TCs.

The initial intensity error ranged up to a maximum of 7 and 9 knots from cold- and cyclic-start VI experiments, respectively. The cyclic initialization exhibited more skill in representing the vertical and horizontal structures of the initial TC vortex. For example, the initial vortex for TC Lehar valid at

00:00 UTC 26 November 2013 from the cyclic experiment produced a distinctly decoupled vortex that leads to the rapid weakening. Most of the time, the cyclic initialization succeeded in correcting the initial vortex of the GFS global analyses with realistic asymmetry. At the same time, the cold initialization/experiment was not able to reproduce the asymmetry (as also seen in Osuri et al., 2017). The initial negative intensity error in cyclic initialization was mainly due to the TC Nargis case, and the possible reasons will be studied in the future.

Interestingly, the cyclic experiment's track error statistics have shown considerably fewer errors up to 2 days. At 48+ h, the model physics and dynamics helped the cold experiment skill to "catch up" to the cyclic experiment skill, and to become positive at the 72-h forecast. However, the cyclic experiment was highly skillful for track and intensity (up to 72-h forecast) compared with the operational forecast and WRF model. The cyclic vortex initialization experiment has shown better performance in representing the time evolution of equivalent potential temperature (θ_e) . The ventilation effect (intrusion of dry air) in the middle layers of the TC Lehar environment was realistically reproduced in the cyclic experiment, and the rapid decay of the TC Lehar was well captured. The cloud condensate also correlated with the intensity, as seen in TC Phailin (higher amounts) and TC Lehar (lesser amounts). The cyclic experiment could show increased amounts of cloud condensate at the actual onset of RI. The cyclic initialization experiment's positive skill could be attributed to the cycled fields of three-dimensional winds, temperature, and moisture in the data-sparse open waters. Thus, the cyclic-start experiment was especially crucial for 2-day forecasts. This finding is relevant to forecast intensity changes as a cyclone nears land correctly.

This study showed that vortex initialization helps the TC forecasting system in a data-sparse region such as the Bay of Bengal (as well as the North Indian Ocean). This method would be a valuable addition to the high-resolution TC models over this region. The performance of cyclic initialization (particularly for longer lead times) could be further improved by assimilating the conventional and nonconventional data sets (Busireddy et al., 2019; Nadimpalli et al., 2020; Osuri et al., 2012, 2015;

Routray et al., 2016), realistic representation of land surface conditions (Niyogi et al., 2016; Osuri et al., 2020), and coupling with appropriate ocean models (Mohanty et al., 2018).

Acknowledgements

This work was supported by a grant from the Indian National Centre for Ocean Information Services (INCOIS). The second author acknowledges the financial support from SERB (ECR/2016/001637), Department of Science and Technology (DST), Govt. of India, and Earth System Science Organization, Ministry of Earth Sciences (MoES/16/14/2014-RDEAS), Government of India. The authors also acknowledge the Indo-US Science and Technology Forum (IUSSTF) for the Indo-US collaboration and IMD for providing observed track and wind speed for validation of model simulation results. Dr. Naveen G and Ms. Dallas Staley are acknowledged for their help in improving the readability of the manuscript. We sincerely acknowledge the reviewers for insightful and constructive comments to improve the quality of the work. This research was supported by the National Science Foundation (Grant AGS-0847472).

Publisher's Note Springer Nature remains neutral with regard to jurisdictional claims in published maps and institutional affiliations.

REFERENCES

Bhalachandran, S., Nadimpalli, R., Osuri, K. K., Marks, F. D., Jr., Gopalakrishnan, S., Subramanian, S., Mohanty, U. C., & Niyogi, D. (2019). On the processes influencing rapid intensity changes of tropical cyclones over the Bay of Bengal. *Scientific Reports*, 9(1), 3382.

Busireddy, N. K. R., Nadimpalli, R., Kumar, A., Osuri, K. K., & Mohanty, U. C. (2019). Impact of vortex size and Initialization on prediction of landfalling tropical cyclones over Bay of Bengal. *Atmospheric Research*, 224, 18–29.

Cha, D. H., & Wang, Y. (2013). A dynamical initialization scheme for real-time forecasts of tropical cyclones using the WRF model. *Monthly Weather Review*, 141(3), 964–986.

Das, A. K., Rao, Y. R., Tallapragada, V., Zhang, Z., Bhowmik, S. R., & Sharma, A. (2015). Evaluation of the Hurricane Weather Research and Forecasting (HWRF) model for tropical cyclone

- forecasts over the North Indian Ocean (NIO). *Natural Hazards*, 75, 1205–1221.
- Davidson, N. E., Xiao, Y., Ma, Y., Weber, H. C., Sun, X., Rikus, L. J., Kepert, J. D., Steinle, P. X., Dietachmayer, G. S., Lok, C. C., & Fraser, J. (2014). ACCESS-TC: Vortex specification, 4DVAR initialization, verification, and structure diagnostics. *Monthly Weather Review*, 142, 1265–1289.
- Davis, C., & Low-Nam, S. (2001). The NCAR-AFWA tropical cyclone bogussing scheme. Air Force Weather Agency (AFWA) Rep, 12.
- Fiorino, M., Goerss, J. M., Jensen, J. J., & Harrison, E. J. Jr. (1993). An evaluation of the real-time tropical cyclone forecast skill of the Navy Operational Global Atmospheric Prediction System in the western North Pacific. Weather and Forecasting, 8, 3–24.
- Gopalakrishnan, S. G., Goldenberg, S., Quirino, T., Zhang, X., Marks, F., Jr., Yeh, K. S., Atlas, R., & Tallapragada, V. (2012). Toward improving high-resolution numerical hurricane forecasting: Influence of model horizontal grid resolution, initialization, and physics. Weather and Forecasting, 27, 647–666.
- Hack, J. J., & Schubert, W. H. (1986). Nonlinear response of atmospheric vortices to heating by organized cumulus convection. *Journal of the Atmospheric Sciences*, 43(15), 1559–1573.
- Heming, J. T., Chan, J. C. L., & Radford, A. M. (1995). A new scheme for the initialization of tropical cyclones in the UK Meteorological Office global model. *Meteorological Applications*, 2, 171–184.
- Hendricks, E. A., Peng, M. S., Ge, X., & Li, T. (2011). Performance of a dynamic initialization scheme in the Coupled Ocean-Atmosphere Mesoscale Prediction System for Tropical Cyclones (COAMPS-TC). Weather and Forecasting, 26(5), 650–663.
- Hodges, K., Cobb, A., & Vidale, P. L. (2017). How well are tropical cyclones represented in reanalysis datasets? *Journal of Climate*, 30(14), 5243–5264.
- Iwasaki, T., Nakano, H., & Sugi, M. (1987). The performance of typhoon track prediction model with cumulus parameterization. *Journal of the Meteorological Society of Japan*, 65, 555–570.
- Kreiss, H. O., & Lorenz, J. (2004). Initial-Boundary Value Problems and the Navier-Stokes Equations, 1989. Reprint SIAM CLASSICS.
- Kurihara, Y., Bender, M. A., & Ross, R. J. (1993). An initialization scheme of hurricane models by vortex specification. *Monthly Weather Review*, 121(7), 2030–2045.
- Kurihara, Y., Bender, M. A., Tuleya, R. E., & Ross, R. J. (1990).
 Prediction experiments of Hurricane Gloria (1985) using a multiply nested movable mesh model. *Monthly Weather Review*, 118(10), 2185–2198.
- Kurihara, Y., Bender, M. A., Tuleya, R. E., & Ross, R. J. (1995).
 Improvements in the GFDL hurricane prediction system.
 Monthly Weather Review, 123(9), 2791–2801.
- Kwon, I. H., & Cheong, H. B. (2010). Tropical cyclone initialization with a spherical high-order filter and an idealized threedimensional bogus vortex. *Monthly Weather Review*, 138(4), 1344–1367.
- Leslie, L. M., & Holland, G. J. (1995). On the bogussing of tropical cyclones in numerical models: A comparison of vortex profiles. *Meteor. Atmos. Phys.*, 56(1–2), 101–110.
- Liu, J., Yang, S., Ma, L., Bao, X., Wang, D., & Xu, D. (2013). An Initialization scheme for tropical cyclone numerical prediction by enhancing humidity in deep-convection region. *Journal of Applied Meteorology and Climatology*, 52(10), 2260–2277.

- Liu, Q., Zhang, X., Tong, M., Zhang, Z., Liu, B., Wang, W., et al. (2020). Vortex initialization in the NCEP operational hurricane models. *Atmosphere*, 11(9), 968.
- Lord, S.J., (1991). A bogusing system for vortex circulations in the National Meteorological Center global forecast model. Preprints, 19th Conf. on Hurricanes and Tropical Meteorology, Miami, FL, Amer. Meteor. Soc., 328–330.
- Mathur, M. B. (1991). The National Meteorological Center's quasi-Lagrangian model for hurricane prediction. *Monthly Weather Review*, 109, 1419–1447.
- Mohanty, S., Halliwell, G.R., Gopalakrishnan, S.G., Dong, J., Kim, H.S., Marks, F.D. and Mohanty, U.C., (2018). Impact of different ocean conditions present in the Bay of Bengal on coupled TC intensity prediction. 33rd Conference on Hurricanes and Tropical Meteorology, Ponte Vedra, FL, USA, 15–20 April 2018.
- Mohanty, U. C., Nadimpalli, R., Mohanty, S., & Osuri, K. K. (2019). Recent advancements in prediction of Tropical Cyclone track over North Indian Ocean basin. *Mausam*, 70(1), 57–70.
- Mohanty, U. C., Osuri, K. K., & Pattanayak, S. (2013). A study on high resolution mesoscale modeling systems for simulation of tropical cyclones over the Bay of Bengal. *Mausam*, 64, 117–134.
- Mohanty, U. C., Osuri, K. K., Tallapragada, V., Marks, F. D., Pattanayak, S., Mohapatra, M., Rathore, L. S., Gopalakrishnan, S. G., & Niyogi, D. (2015). A Great Escape from the Bay of Bengal "Super Sapphire-Phailin" Tropical Cyclone—A case of improved weather forecast and societal response for disaster mitigation. *Earth Interactions*, 19(17), 1–11.
- Mohapatra, M., Nayak, D. P., Sharma, R. P., & Bandyopadhyay, B. K. (2013a). Evaluation of official tropical cyclone track forecast over north Indian Ocean issued by India Meteorological Department. *Journal of Earth System Science*, 122(3), 589–601.
- Mohapatra, M., Bandyopadhyay, B. K., & Nayak, D. P. (2013b). Evaluation of operational tropical cyclone intensity forecasts over north Indian Ocean issued by India Meteorological Department. *Natural Hazards*, 68(2), 433–451.
- Nadimpalli, R., Osuri, K. K., Mohanty, U. C., Das, A. K., Kumar, A., Sil, S., & Niyogi, D. (2019). Forecasting Tropical Cyclones in the Bay of Bengal using quasi-operational WRF and HWRF modeling systems: An assessment study. *Meteorology and Atmospheric Physics*. https://doi.org/10.1007/s00703-019-00669-6
- Nadimpalli, R., Srivastava, A., Prasad, V. S., Osuri, K. K., Das, A. K., Mohanty, U. C., & Niyogi, D. (2020). Impact of INSAT-3D/3DR radiance data assimilation in predicting Tropical Cyclones over North Indian Ocean region. *IEEE Transactions on Geoscience and Remote Sensing*. https://doi.org/10.1109/TGRS. 2020.2978211
- Niyogi, D., Subramanian, S., & Osuri, K. K. (2016). The role of land surface processes on Tropical Cyclones: Introduction to Land Surface Models. In U. C. Mohanty & S. G. Gopalakrishnan (Eds.), Advanced numerical modeling and data assimilation techniques for Tropical Cyclone prediction (pp. 221–246). Dordrecht: Springer.
- Nolan, D. S., Miyamoto, Y., Wu, S. N., & Soden, B. J. (2019). On the correlation between total condensate and moist heating in tropical cyclones and applications for diagnosing intensity. *Monthly Weather Review*, 147(10), 3759–3784.
- Nolan, D. S., Moon, Y., & Stern, D. P. (2007). Tropical cyclone intensification from asymmetric convection: Energetics and efficiency. *Journal of the Atmospheric Sciences*, 64(10), 3377–3405.

- Osuri, K. K., Mohanty, U. C., Routray, A., & Mohapatra, M. (2012). Impact of Satellite Derived Wind Data Assimilation on track, intensity and structure of tropical cyclones over North Indian Ocean. *International Journal of Remote Sensing*, 33(5), 1627–1652.
- Osuri, K. K., Mohanty, U. C., Routray, A., Mohapatra, M., & Niyogi, D. (2013). Real-time track prediction of tropical cyclones over the North Indian Ocean using the ARW model. *Journal of Applied Meteorology and Climatology*, 52(11), 2476–2492.
- Osuri, K. K., Mohanty, U. C., Routray, A., & Niyogi, D. (2015). Improved prediction of Bay of Bengal Tropical Cyclones through assimilation of Doppler weather radar observations. *Monthly Weather Review*, 143, 4533–4560.
- Osuri, K. K., Nadimpalli, R., Ankur, K., Nayak, H. P., Mohanty, U. C., Das, A. K., & Niyogi, D. (2020). Improved simulation of monsoon depressions and heavy rains from direct and indirect initialization of soil moisture over India. *Journal of Geophysical Research: Atmospheres*, 125(14), e2020JD032400.
- Osuri, K. K., Nadimpalli, R., Mohanty, U. C., & Niyogi, D. (2017).
 Prediction of rapid intensification of tropical cyclone Phailin over the Bay of Bengal using the HWRF modelling system.
 Quarterly Journal Royal Meteorological Society, 143, 678–690.
- Peng, M. S., Jeng, B. F., & Chang, C. P. (1993). Forecast of typhoon motion in the vicinity of Taiwan during 1989–90 using a dynamical model. Weather and Forecasting, 8, 309–325.
- Prasad, K., & Rao, Y. R. (2003). Cyclone track prediction by quasi-Lagrangian limited area model. *Meteorology and Atmospheric Physics*, 83, 173–185.
- Pu, Z. X., & Braun, S. A. (2001). Evaluation of bogus vortex techniques with four-dimensional variational data assimilation. *Monthly Weather Review*, 129(8), 2023–2039.
- Routray, A., Mohanty, U. C., Osuri, K. K., Kar, S. C., & Niyogi, D. (2016). Impact of satellite radiance data on simulations of Bay of Bengal tropical cyclones using the WRF-3DVAR modeling system. *IEEE Transactions on Geoscience and Remote Sensing*, 54(4), 2285–2303.
- RSMC report. (2014). Report on cyclonic disturbances over North Indian Ocean during 2014, No. ESSO/IMD/RSMC-Tropical Cyclones Report No. 01 (2015)/6.
- Sandeep, S., Chandrasekar, A., & Singh, D. (2006). The impact of assimilation of AMSU data for the prediction of a tropical cyclone over India using a mesoscale model. *International Journal of Remote Sensing*, 27(20), 4621–4653.
- Singh, R., Kishtawal, C. M., Pal, P. K., & Joshi, P. C. (2012). Improved tropical cyclone forecasts over north Indian Ocean with direct assimilation of AMSU-A radiances. *Meteorology and Atmospheric Physics*, 115(1–2), 15–34.
- Singh, R., Pal, P. K., Kishtawal, C. M., & Joshi, P. C. (2008). The impact of variational assimilation of SSM/I and OuikSCAT

- satellite observations on the numerical simulation of Indian Ocean tropical cyclones. *Weaather and Forecasting*, 23(3), 460–476.
- Storer, R. L., Zhang, G. J., & Song, X. (2015). Effects of convective microphysics parameterization on large-scale cloud hydrological cycle and radiative budget in tropical and midlatitude convective regions. *Journal of Climate*, 28, 9277–9297.
- Tallapragada, V. (2016). Overview of the NOAA/NCEP operational Hurricane Weather Research and Forecast (HWRF) modelling system. In Advanced Numerical Modeling and Data Assimilation Techniques for Tropical Cyclone Prediction (pp. 51–106). Dordrecht: Springer.
- Tallapragada, V., and Coauthors. (2013). Hurricane Weather and Research and Forecasting (HWRF) Model: 2013 scientific documentation. Development Testbed Center Doc., 99 pp. www. dtcenter.org/HurrWRF/users/docs/scientific_documents/ HWRFv3.5a_ScientificDoc.pdf.
- Tallapragada, V., Kieu, C., Kwon, Y., Trahan, S., Liu, Q., Zhang, Z., & Kwon, I. (2014). Evaluation of storm structure from the operational HWRF model during 2012 implementation. *Monthly Weather Review*, 142, 4308–4325.
- Tallapragada, V., Kieu, C., Trahan, S., Zhang, Z., Liu, Q., Wang, W., & Strahl, B. (2015). Forecasting Tropical Cyclones in the Western North Pacific Basin using the NCEP operational HWRF: Real-time implementation in 2012. Weather and Forecasting, 30(5), 1355–1373.
- Tang, B., & Emanuel, K. (2010). Midlevel ventilation's constraint on tropical cyclone intensity. *Journal of Atmospheric Science*, 67, 1817–1830.
- Trinh, V. T., & Krishnamurti, T. N. (1992). Vortex initialization for typhoon track prediction. *Meteorology and Atmospheric Physics*, 47(2–4), 117–126.
- Ueno, M. (1995). A study on the impact of asymmetric components around tropical cyclone center on the accuracy of bogus data and the track forecast. *Meteorology and Atmospheric Physics*, 56, 125–134.
- Wang, Y. (1998). On the bogusing of tropical cyclones in numerical models: The influence of vertical structure. *Meteorology and Atmospheric Physics*, 65(3–4), 153–170.
- Wu, L., Tian, W., Liu, Q., Cao, J., & Knaff, J. A. (2015). Implications of the observed relationship between tropical cyclone size and intensity over the Western North Pacific. *Journal of Climate*, 28, 9501–9506. https://doi.org/10.1175/JCLI-D-15-0628.1
- Zou, X., Qin, Z., & Zheng, Y. (2015). Improved tropical storm forecasts with GOES-13/15 imager radiance assimilation and asymmetric vortex initialization in HWRF. *Monthly Weather Review*, 143(7), 2485–2505.